8. PRÁCE AUTORA IN EXTENSO

Epilepsia, **44**(5):636–639, 2003
Blackwell Publishing, Inc.

Short Bursts of Weak Pulses Break Postictal Inhibition in the Neocortex of Wistar Rats

Lukáš Tůma, David Krýsl, and Jan Mareš

Department of Normal, Pathological and Clinical Physiology, Charles University, Third Faculty of Medicine, Prague, Czech Republic

Summary: *Purpose:* Postictal inhibition (PI) is a decrease in excitability that follows an epileptic seizure and decreases probability of new seizure occurrence. PI may involve both increased inhibition and persisting elevated excitation. Our experiments tested whether shorter trains of weak stimuli are able to unmask this residual increase of excitability during the PI.

Methods: Four epileptic afterdischarges (ADs) were evoked by intense electrical stimulation (20 s, 8 Hz, current intensity at 5× threshold) of the neocortex in two groups (A, B) of Wistar rats. Before the first AD and during the 10-min interictal period, 8-Hz trains of four weak pulses (half of the intensity used for the AD triggering; 4P) were applied every 20 s in group B and a single pulse with similar parameters in group A.

Results: The number of interictal epileptiform events evoked by 4P in the group B was significantly higher than that in the group A (evoked by single pulses) except after the second AD. Epileptic events were triggered by 4P also immediately after the AD termination.

Conclusions: It is apparent that weak stimulation can trigger epileptic phenomena during PI. Our results indicate that it is no longer possible to perceive PI only as persisting extreme and active inhibition. An appropriate stimulation can reveal more subtle (but important) excitatory events contributing to the functional status during the postictal period. **Key Words:** Epilepsy—Postictal inhibition—Electrical stimulation—Rat—Kindling—Seizure.

Epileptic seizures are usually followed by a period when it is difficult or impossible to evoke any seizure. This postictal inhibition (PI) occurs also after seizures elicited by electrical stimulation. If the same stimulation parameters are used in an attempt to evoke an epileptic afterdischarge (AD) during the PI, the AD cannot be elicited (1,2). A broad spectrum of changes in CNS function such as altered behavior, modification of EEG (3,4), evoked potentials (5), and also molecular changes (6–8) were documented during the PI. Among the mechanisms involved in seizure termination, a massive active inhibition is widely believed to play the main role (9,10). However, some experimental evidence points to a more complex view of events during the PI [for example, changes in energetic metabolism (8) or decreased number of synaptic vesicles (11)].

Mechanisms leading to the PI are apparently activated during the seizure, and they can be involved in seizure termination. However, in some experiments, spontaneous acute recurrent ADs were observed when PI normally occurs. This phenomenon was observed in adult as well as in young rats (12). The mechanisms involved in seizure termination also are obviously insufficient during status epilepticus (SE) (10). These may indicate persisting increase in excitability during the development of the PI. For the testing of seizure susceptibility during the PI, an intense stimulation is commonly used (1,7). It is based on the concept that such stimulation should overrun the PI.

Our hypothesis anticipates the coexistence of increased excitability with persisting activation of inhibitory factors during the postictal period. In this study, we tested whether certain stimulation paradigms could unmask residual excitability during the PI. We determined whether a burst (8 Hz) of four pulses (4P) weaker than those used to elicit ADs, applied during the interictal period, may evoke ictal phenomena. We also tested whether the administration of 4P affects the induction of the next AD.

METHODS

Adult male Wistar rats (N = 18) were randomly assigned to two groups (A, B) of nine. All experiments were carried out on freely moving animals.

Accepted November 17, 2002.
Address correspondence and reprint requests to Dr. J. Mareš at Department of Normal, Pathological and Clinical Physiology, 3rd Fac Med, Charkles University, Ke Karlovu 4, 120 00 Praha 2, Czech Republic. E-mail: jan.mares@lf3.cuni.cz

Surgery

Under pentobarbital (PTB) anesthesia (70 mg/kg, intraperitoneally) bipolar stimulation electrodes were placed on the right sensorimotor (SM) area and registration electrodes on both SM areas and on the visual cortex. An indifferent electrode was positioned on the nasal bone. All electrodes were fixed in their places with a cap composed of acrylic.

Experiment

One week after surgery, the rats were connected to the computer-based EEG recorder, and 5 min of spontaneous electrocorticography (ECoG) was recorded in each animal. Threshold for an evoked potential (interhemispheric response) was estimated by increasing the intensity of individual pulses stepwise (10 μA). When five subsequent evoked potentials were detected with a given intensity, then the previous level of intensity was accepted as a threshold and used as a reference value (RI) for stimulation intensity. Two types of interictal stimulation were used: single bipolar rectangular pulses (intensity at 2.5× RI; duration, 1 ms; and interstimulation interval, 20 s); and 4P (train of four pulses with the frequency of 8 Hz, intensity at 2.5× RI). After the end of the reference intensity estimation, 20 single pulses were administered in group A, and 20 4P, in group B.

This was followed by triggering of four ADs in each animal (stimulation, 8 Hz; intensity, 5× RI; duration of the stimulation train, 20 s; pulse duration, 1 ms). This stimulation paradigm was much more intense than either of the previously mentioned types of interictal stimulations. Intervals between ADs evoked by intense stimulations lasted 10 min. During these intervals, single pulses (in group A) and 4Ps (in group B) with the same parameters as for the pre-AD stimulation were administered 4P (See the sequence of stimulations for both groups in Fig. 1A.) During the ADs, behavior of the animals was observed and recorded with special attention to the occurrence of loss of balance (LB; falling). The presence or absence of LB was used to estimate the behavioral severity of the ADs. The duration of individual ADs was measured.

Statistical evaluation

To compare the number of interictal epileptic phenomena in group A with the number of interictal epileptic phenomena in group B, the Mann–Whitney *U* test was used. The differences between the groups in the mean AD duration after the first, second, third, and fourth intense stimulations were tested by using Student's *t* test. The total number of ADs with LB after the first, second, third, and fourth intense stimulations was compared between the groups by using the χ^2 test. Level of significance was always preset to $p < 0.05$.

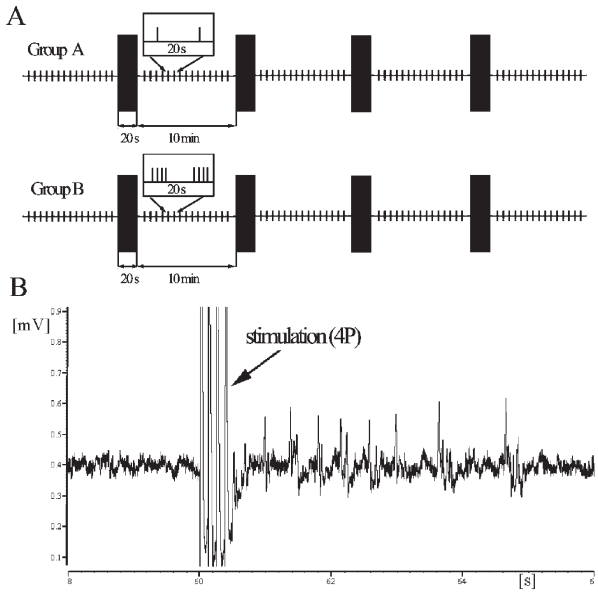

FIG. 1. **A:** Scheme of the stimulation protocol. **B:** Short seizure elicited by four weak pulses (8 Hz) after the end of the afterdischarge

RESULTS

In group A, single pulses did not evoke any epileptiform activity before the induction of the first AD (i.e., in the animal without a history of seizures). In group B, the 4P evoked atypical EEG response in one of nine animals before the induction of the first AD.

In group A ($n = 9$) after any of the four ADs, single pulses evoked only a few short seizures. However, the number of short seizures (Figs. 1B and 2) associated with 4P (group B; $n = 9$), when compared with single pulses in group A, was significantly higher after the first ($p < 0.05$), third ($p < 0.05$), and fourth (Student's *t* test; $p < 0.05$), but not after the second AD (Fig. 3). The total number of evoked short seizures was significantly higher in group B (Mann–Whitney *U* test, $p < 0.01$).

FIG. 2. Mean number of short seizures elicited by stimulations before (control) and after afterdischarges (±SEM). In group A, single pulses at 20-s intervals were used, and in group B, trains of four pulses at 8 Hz were applied (*$p < 0.05$).

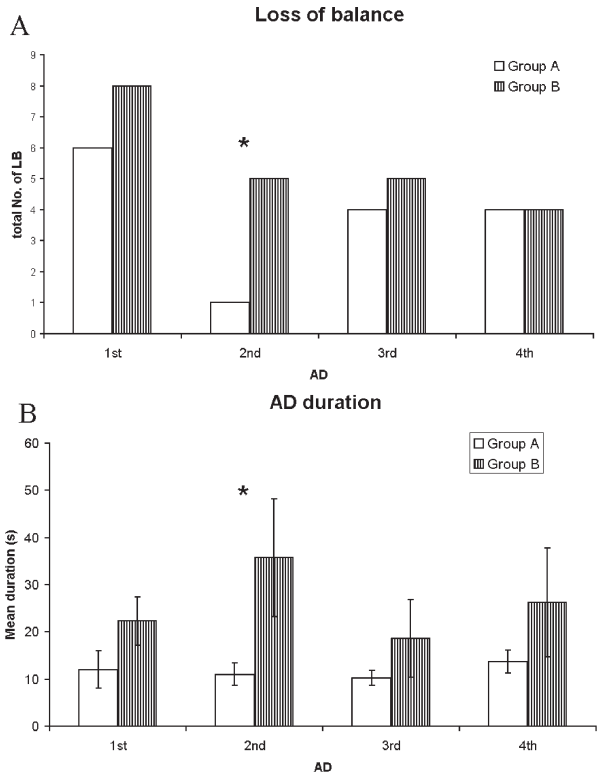

FIG. 3. Comparison of subsequent epileptic afterdischarges (ADs) between the groups. **A:** Number with loss of balance. **B:** Mean duration of ADs (±SEM) (*$p < 0.05$).

Mean duration of the second AD in group B was significantly longer compared with the mean duration of the second AD in group A ($p < 0.05$). ADs after the first, third, and fourth intense stimulations did not differ significantly between the groups when comparing mean durations. No difference in the duration of the four consecutive ADs was found within each group (Fig. 3).

Significantly more ADs were associated with falling of the animal (LB, Fig. 3) after the second AD in group B compared with the second AD of group A (χ^2 test, $p < 0.05$). However, comparison of absolute numbers with falling between both groups yielded no significant differences.

DISCUSSION

From our previous experiments (1) and other reports (13), it is known that the strong stimulation (used to elicit ADs) is not able to trigger a new AD during the initial phases of the PI. In the present experiment, the trains of only four weak pulses (4P) were able to trigger more short seizures immediately after the AD. The single pulses were too weak to elicit epileptic phenomena in more animals. Some differences between the groups in LB occurrence were noted, which tended to be higher in the group subjected to interictal stimulation with four pulses. Prolongation of ADs (acute kindling) was not observed in any group.

We were able to trigger new short seizures during the postictal period, if an appropriate stimulation paradigm was chosen. Stimulated SM cortex did not display relative or absolute refractoriness in terms of resistance to both types of stimuli with lower intensity (single pulses or 4P). Trains of four stimuli were able to trigger epileptic phenomena more often than single pulses during the PI after ADs in our experiments. No difference in AD duration, EEG pattern, or behavioral severity of seizures was found in the first AD when comparing group A with group B. Given that the first AD was similar in group A and group B, we can hypothesize that the postictal period also was similar; thus we can assume that short seizures evoked in the postictal period were caused by an acute direct influence of 4P on neuronal excitability. We cannot rule out some long-lasting effects of 4Ps on excitability, but in our experiment, the occurrence of short seizures does not seem to be a consequence of changes induced by 4P during the preceding AD in naive animals.

The parameters of the stimulation used in our previous work (1) to trigger AD and test the duration of the PI were the same as in the intense stimulation in the present experiment. It was shown (1,13) that the application of the same type of intense stimulation that was used to elicit ADs (i.e., intense stimulation) leads to clear signs of PI during the first minutes after the end of the previous AD. This was not the case when weak stimuli (4P) were used. An explanation involves at least two processes participating in the PI. We propose that a hidden increase in activity of the excitatory system persists on the background of active inhibition and synaptic exhaustion (10,11).

Our short seizures may appear on the background of evoked oscillations in excitability (14). This is supported by the result of the experiment (12), in which stimulations of greater intensity and frequency (50 Hz) and short duration (2 s) were used to evoke ADs, and the occurrence of spontaneous recurrent seizures was described. A short train of weak pulses may enhance excitability increased by the previous AD by mechanisms similar to those anticipated in paired-pulse stimulation.

Although our data do not provide more information about involved mechanisms, it is tempting to compare our results with the recent findings in the hippocampus. Partial explanation of our results is similar to the discussed theory of "irritable mossy cell" (15). In acute experiments, such as our study, it is unlikely that the cell death would be responsible for the epileptic events observed. More likely, functional impairment of excitatory and inhibitory interneurons could be the main culprit. In the hippocampus, mossy cells respond to depolarization with an increase in excitability [reflected in sharp excitatory postsynaptic potentials (EPSPs)]. If the 4P

exerted such an effect on a functionally similar neuronal system and/or a transient impairment of inhibitory interneuron function, the net effect could be the occurrence of short afterdischarges detectable on the ECoG. Another intense stimulation delivered after the AD termination would suppress "irritable" cells and also support activity of the inhibitory systems.

In our present experiment, both types of weak stimulation before the first AD and during the interictal period influenced subsequent seizures. This phenomenon was especially emphasized when the 4Ps were used. Significantly longer ADs after the second intense stimulation were observed in group B in comparison to group A. Occurrence of LB also was higher in the group B. However, AD repetitions in the neocortex did not lead to the AD prolongation (acute kindling) [see (1)]. Observed differences could be related to stimulation paradigms in groups A and B.

We suppose that the stimulation during the PI may play a role in acute kindling manifestation. Conversely, not only the seizure but also the presence of PI may be important for the kindling phenomenon. However, the relation between acute kindling and PI does not have to be direct.

Our results show that during the PI, it is possible to evoke or unmask increased excitability concealed by activated proinhibitory systems in this period. Attempts to elicit a seizure by intense stimulation may paradoxically act more to accentuate inhibitory factors than to increase excitability. In such a case, the result of stimulation is reinforcement of refractoriness.

Our results contribute to the explanation of mechanisms involved in the development of SE. On the basis of all the new evidence, the concept of the postictal period should be revised.

Acknowledgment: This study was supported by grants GA UK 98/1999/C, HEDF 1815 F3, and Ministry of Education J13/98:111100005.

REFERENCES

1. Mareš J, Mareš P, Kadlecová-Jursíková D. Changes in the excitability of rat cerebral cortex after a self-sustained after-discharge. *Electroencephalogr Clin Neurophysiol* 1982;53:283–8.
2. Swartzwelder HS, Wegener ST, Johnson CT, et al. Depressed excitability and integrated EEGs following hippocampal afterdischarges. *Brain Res Bull* 1980;5:509–17.
3. Aldenkamp AP. Effect of seizures and epileptiform discharges on cognitive function. *Epilepsia* 1997;38(suppl 1):S52–S5.
4. Daniel WF, Crovitz HF, Weiner RD, et al. ECT-induced amnesia and postictal EEG suppression. *Biol Psychiatry* 1985;20:344–8.
5. Kriss A, Halliday AM, Halliday E, et al. Evoked potentials following unilateral ECT, II: the flash evoked potential. *Electroencephalogr Clin Neurophysiol* 1980;48:490–501.
6. Vanore G, Giraldez L, Rodriguez de Lores Arnaiz G, et al. Seizure activity produces differential changes in adenosine A1 receptors within rat hippocampus. *Neurochem Res* 2001;26:225–30.
7. Velíšek L, Mareš P. Differential effects of naloxone on postictal depression. *Epilepsy Res* 1992;12:37–43.
8. Šťastný F, Mareš J, Trojan S. Rapid modulation of rat cortical Na+-K+-ATPase during recovery following self-sustained afterdischarges. *Physiol Bohemoslov* 1981;30:79–83.
9. Rocha L, Ackermann RF, Engel JJ. Effects of chronic morphine pretreatment on amygdaloid kindling development, postictal seizure and suppression and benzodiazepine receptor binding in rats. *Epilepsy Res* 1996;23:225–33.
10. Young D, Dragunow M. Status epilepticus may be caused by loss of adenosine anticonvulsant mechanisms. *Neuroscience* 1994;58:245–61.
11. Langmeier M, Mareš J, Fischer J. Number of synaptic vesicles in rat cortex immediately after cessation of the self-sustained afterdischarge during kindling. *Epilepsia* 1983;24:616–27.
12. Mareš J, Beneš P, Mareš P, et al. Influence of certain stimulation parameters on the character of the cortical self-sustained afterdischarge. *Physiol Bohemoslov* 1983;32:30–7.
13. Marešová D, Valkounová I, Jandová K, et al. Excitability changes of cortical neurons during the postnatal period in rats exposed to prenatal hypobaric hypoxia. *Physiol Res* 2001;50:215–9.
14. Penttonen M, Nurminen N, Miettinen R, et al. Ultra-slow oscillation (0.025 Hz) triggers hippocampal afterdischarges in Wistar rats. *Neuroscience* 1999;94:735–43.
15. Ratzliff AH, Santhakumar V, Howard A, et al. Mossy cells in epilepsy: rigor mortis or vigor mortis? *Trends Neurosci* 2002;25:140–4.

SEMI-INTERACTIVE DETECTION OF ACTION POTENTIALS USING LOCAL WAVE FEATURES AND CLUSTERING

LUKÁŠ TÛMA[1,2], KLÁRA BERNÁŠKOVÁ[2], JAN MAREŠ[2]
[1]4th Department of Internal Medicine, General Teaching Hospital in Prague, Czech Republic,
[2]Department of Normal, Pathological and Clinical Physiology, 3rd Faculty of Medicine, Charles University in Prague, Czech Republic

Abstract

Impressive achievements in neuronal waveform processing branch into abundant pool of dedicated algorithms - modifications of few core principles. This paper details design and implementation of effective customizable algorithm for detection of extracellularly recorded action potentials demonstrated on recordings from brain cortex of adult male Wistar rats. At first signal is filtered using surroundings amplitude averaging and moving average subtraction. Subsequently, location of data points in which first derivation of waveform crosses zero value steeper than in common artefacts found in background activity is estimated. For description of the point's surroundings, amplitude and steepness with their bilateral symmetry are calculated and utilized to select graphoelements that are subsequently clustered by modified K-means algorithm. This procedure allows formation of shape patterns of action potentials. Comprehensive offline analysis of our recordings demonstrated this approach as well utilizable for typifying and consecutive selection of action potentials, which fluctuate due to experimental interventions. Moreover, it facilitates distinguishing activity of separate neurons in multi-unit waveforms.

Key words: spike detection, clustering, action potential, K-means, neuronal network.

INTRODUCTION

Automated action potential detection and processing constitutes an inherent precondition for modern evaluation and interpretation of all recordings of electrical activity of excitable cells. In our experiment, changes in neuronal activity in cortex of the rat during development of cortical ischemic lesion caused by photothrombotic vessel occlusion were investigated [1, 2, 3, 4, 5]. An electric signal is recorded both from inside and from the vicinity of a developing ischemic focus. Changes in extracellular space are anticipated in our experiments. Therefore, alteration in shape and other characteristics of extracellular activity record of particular neuron can be obviously expected. This may be caused either by response of a cell (and its neighbours) to ischemia or neuron dislocation due to development of perifocal oedema as well as its eventual lysis. The nominal impedance of registration microelectrode determines the capability to register multiple unit activity. Because of mutual displacement of electrode and tissue during recording, more than one type of cell activity can be registered and the shape of action potential may vary in time.

Indisputably, the process of detection and analysis of recordings of action potentials is computationally intensive; sensitivity and specificity enhancement of an algorithm is burdened with increased computational complexity. Respective methods can be divided according to their complexity, the usage of artificial intelligence, fuzzy operators, clustering and the necessity of human interaction during the process of data evaluation. Peak tracking based on sole amplitude is an unsophisticated and simple method with linear time complexity [6, 7]. Employment of shape border constraints [8], or sliding clipping window determining steepness and amplitude of a peak has also been reported. Another method is the Maximum Integral Transform Alignment, which is based on integration of positive and negative part of an action potential [9]. Graphoelements showing little variation in time can be tracked by searching for their characteristic features [6]. Next technique that allows identifying action potentials is filtration. More sophisticated methods use transformation of a signal into another domain: for example wavelet or Fourier transforma-

Address for correspondence:
Lukas Tuma M.D. Ing., Department of Normal, Pathological and Clinical Physiology, 3rd Faculty of Medicine, Charles University in Prague, Czech Republic

tion, both otherwise profusely exploited in multimedia compression [10, 11]. Clustering of similar spikes and principal component analysis facilitate recognition of both outlying values and signals from multiple cells recorded simultaneously in one waveform – multiple unit activity [6, 7, 12]. Rapid progress in computer technology allows implementation of algorithms with growing complexity and accuracy for automated signal evaluation even in real time on machines with affordably priced computational force.

The objective of this work was to invent and implement sufficiently accurate algorithm for tracking and sorting of single unit potentials in recordings of electrical activity of one or a small group of neurons. It was necessary to create an algorithm for off-line evaluation of waveforms recorded within our experimental work. Activity changes in time as an expected response to the experimental intervention had to be considered as well. The algorithm was designed to evaluate 20 minute waveform sampled at 10 kHz in same-order time growing linearly with the number of data points.

Detection of single unit potentials is an especially specific task. Combination of previously mentioned principles is necessary to achieve high-quality results. Furthermore, additional complexity is required to evaluate recordings of varying technical quality.

METHODS

Subjects: The data were recorded in adult male Wistar rats weighing from 200 to 250 g. The animals were raised under a controlled light cycle (12 hours light, 12 hours dark, lights on at 6:00 am) with free access to food and water. All procedures were performed in accordance with Ethical Guidelines of the 3rd Faculty of Medicine, Charles University, and in agreement with Guidelines of the Animal Protection Law of the Czech Republic, which corresponds to respective EU regulations. Ethical Commission approved the experimental protocol. Special care was given to minimize animal suffering. After induction to anaesthesia (Urethane, 20%, 6.5ml/kg, intraperitoneally), the scull was uncovered and two trephine openings 3 mm in diameter were made bilaterally over the somatosensory cortex. A peripheral catheter was inserted into caudal vein and the animal was fixed in a stereotactic apparatus. Glass microelectrodes (impedance 6 × 1.5 M) filled with 3 mol NaCl solution were used for registering the activity of cortical neurons in the right sensorimotor area. Obtained signal was amplified with an operational amplifier with adjustable resistance in the feedback loop. A 16-bit A/C converter Micro 1401 by Cambridge

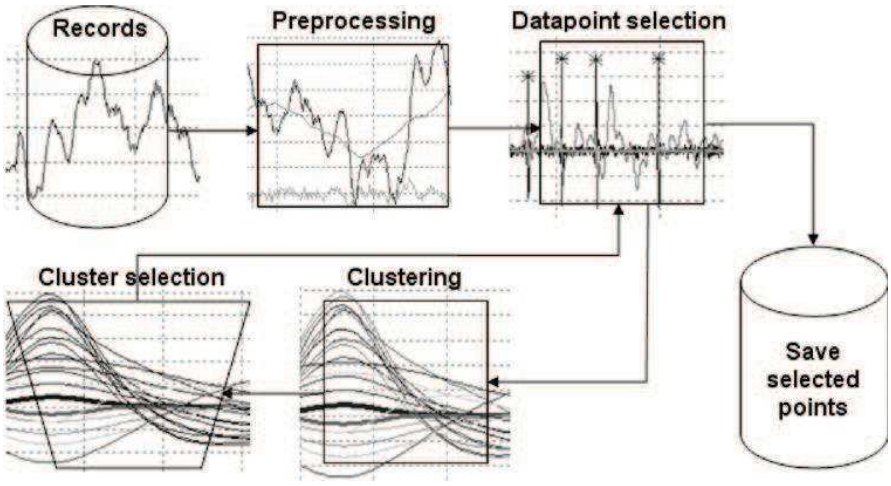

Fig. 1: Algorithm flowchart.

Electronic Design with input range ± 5 V was used for data digititalization. The experiment started with registration of 5 minutes of spontaneous waveform. Afterwards either photosensitive dye Rose Bengal (20 mg/2 ml/kg, dissolved in 0.9 % NaCl) was applied slowly into systemic circulation in the experimental group or saline solution in equal volume in the control group. Subsequently a diode laser irradiation was used as a light source for photothrombosis (duration 9 minutes, wavelength 532 nm, power density 50 mW/mm^2, illuminated area < 1 mm^2). After that, recording continued for another 11 minutes.

Algorithm: The algorithm was implemented in C++, which was chosen for its simplicity, versatility and effective code generation. The recordings were processed on a PC running on AMD Sempron 3000+ mobile processor with 512 MB of RAM. We decided to implement a three-phase waveform evaluation procedure (Fig. 1).

First phase: Initially, the waveform is preprocessed. Low frequencies are eliminated by subtraction of moving average from the waveform (Fig. 2a). Duration of the base of sliding average is at least three times longer than the expected duration of an action potential, which attains in our case typically 12 points, i.e. 1.2 ms. A 36 points long base yields cut-off frequency around 100 Hz. Waveform smoothing and filtering off a high-frequency noise is achieved by substitution of a data point with an average of its surroundings with a typical size of ± 0.1 ms i.e. ± 1 data point in our particular case (Fig. 2b).

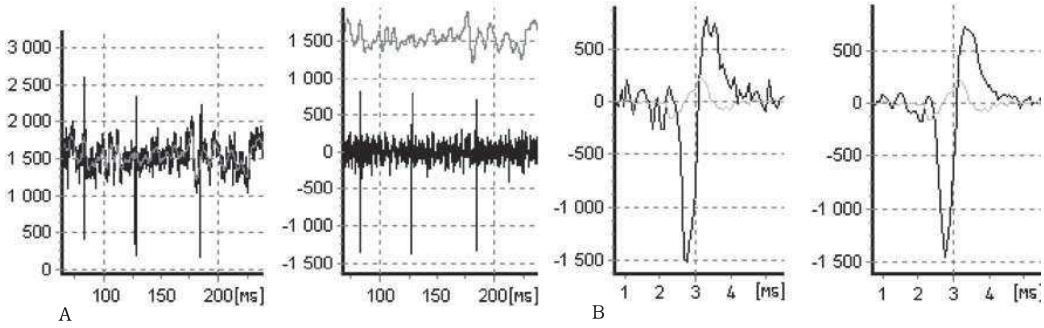

Fig. 2. A: Moving average – a highpass filter: original waveform (black) and moving average (grey) on the left; filtered signal (black) and subtracted moving average (grey) on the right.
B: Neighborhood averaging – a lowpass filter: original waveform (black) and steepness (grey) on the left, smoothed waveform (black) on the right.

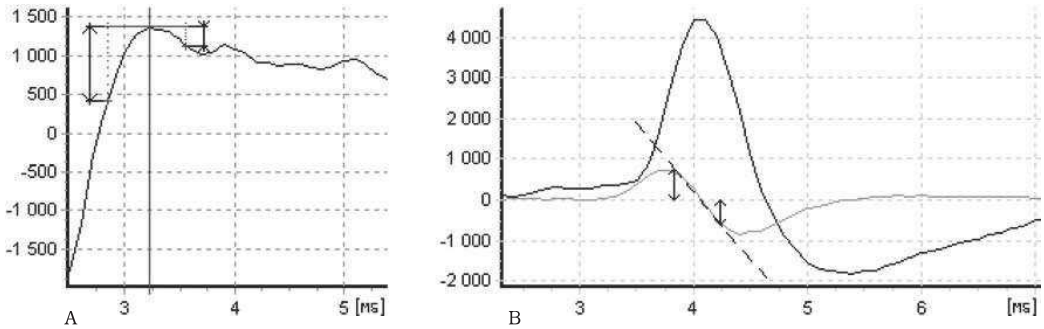

Fig. 3. A: Asymmetry of the data point neighborhood: waveform (black), arrowheads delineate amplitude variation in constant time interval that corresponds with wave asymmetry.
B: Steepness of the data point neighborhood: original waveform (black), steepness (grey). Arrowheads delineate steepness variation in constant time interval.

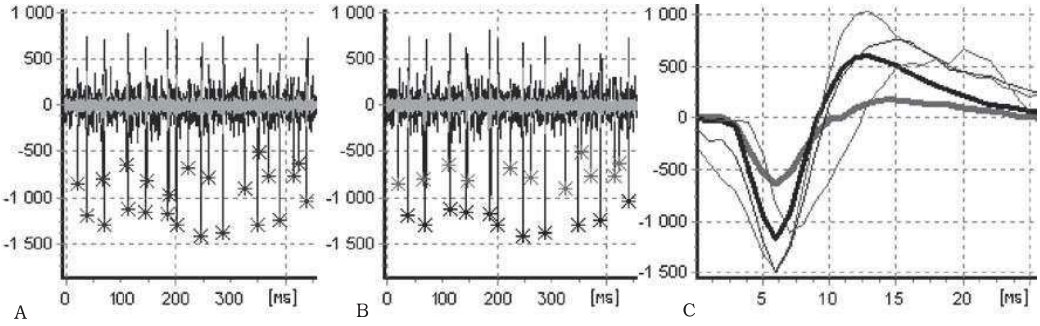

Fig. 4. A: Preselected action potentials: preprocessed waveform (black) with preselected points marked with stars (*). B: Action potentials matched to cluster patterns: preprocessed waveform (black) with preselected points marked with stars (*), the two colors distinguish two clusters.waveform (black). C: Clusters matching action potentials in Figure 4b.

Second phase: The objective of the second part of waveform processing is to reduce the number of points entering the third, the most computationally demanding part to minimum. We search the points that resemble action potentials in their features or in features of their surroundings. Points embodying defined characteristics mark most likely spikes we are looking for. Amplitude, steepness (Fig. 3a) and symmetry (Fig. 3b) were chosen as the most helpful to differentiate action potential from other activity. Both amplitude and steepness are considered as upper boundary values for the background noise and are calculated from the data point surroundings with adjustable size, typically ± 5 data points, i.e. ± 0.5 ms in our particular case. The symmetry criterion determines the maximal ratio of amplitude or steepness before and after particular data point, thus excluding usually asymmetric artefacts. Common values range from 0.1 to 10-fold. At the end of the second part, the set of „interesting" points contains only a fraction of its initial size (Fig. 4a).

Third phase: The last part, the clustering, is operator dependent. The objective is to assign preselected waves (the output from the second part) to a defined number of the closest patterns. This allows to pinpoint the time variability of action potentials or to distinguish activity of multiple cells. For clustering, modified K-means algorithm was chosen [9, 12, 13, 14, 15, 16]. The algorithm assigns particular vectors $\boldsymbol{x}_1, \boldsymbol{x}_2 \ldots \boldsymbol{x}_m$ with n components as data points of action potentials in our case to the closest cluster pattern. The pattern, which has minimal distance from a particular vector, is updated proportionally to its strength (i.e. the number of already associated vectors), so that their mutual distance decreases. This step guarantees convergence of the algorithm as well. The distance between two vectors is defined as:

$$|| \boldsymbol{x}_1, \boldsymbol{x}_2 || = \sum_{i=1}^{n} | x_{1,i} - x_{2,i} |$$

and the closest vector is the only one with minimal distance.

Since the diversity among the patterns can hardly be estimated in advance, the number of patterns is not implicitly dependent on the variance of the spikes, but it is preset by the operator. If the distance of two closest patterns is lower than the distance of the examined vector and its closest pattern, a new pattern originating in the particular vector is created.

If the number of patterns exceeds the limit initially set by the operator, the two closest merge proportionally to their respective strength. Further destiny of the patterns is interactively determined by the operator considering their shape and number of associated spikes, as displayed on the screen. Vectors that were associated with undesired patterns can be easily erased. Clustering and selection can be iterated and so can clusters be divided into even smaller subsets (Fig. 4b and 4c). The third part is the most computationally demanding one: the time complexity rises about linearly with the number of preselected data points and less than exponentially with the

number of patterns. The computation time can be improved by limiting the number of clusters usually to 10 to 20.

RESULTS

The developed algorithm was successfully implemented and employed in our experimental work for detection of single unit potentials in recordings counting n = 12 million data points i.e. 20 minutes sampled at 10 kHz. Specificity and sensitivity was tested on signal mixed from artifitial neuron model [17] (Fig. 5a) and uniform background noise recording (Fig. 5b) in respective ratios. The 1:1 ratio (maximal amplitude of generated signal : maximal amplitude of noise) yielded brilliant 0.89% misplaced or missed action potentials (Fig. 5c). The time complexity of the second part (the point preselection) is O(n) and of the third part (the clustering) $O(nv^2)$, where v is the preset number of patterns. The final output of the program is a binary file containing vectors of selected action potentials including their timestamp. Groups of such files are subsequently analyzed in a different environment. The program features output from intermediate stages of the analysis (patterns, selected vectors) in form of a table that can be easily processed in a standard spreadsheet program.

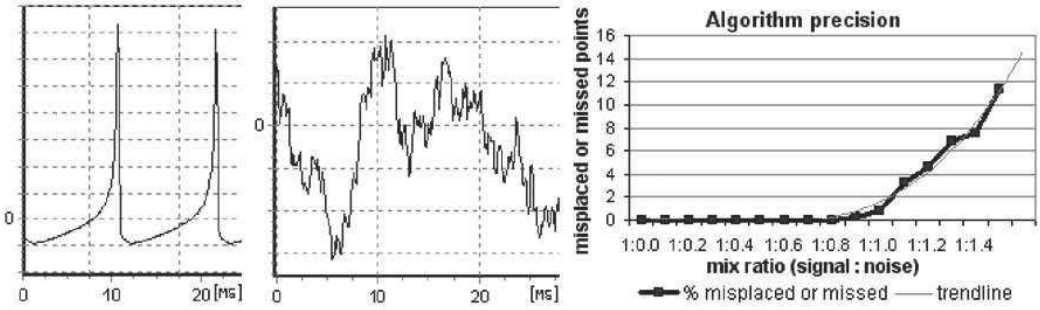

Fig. 5. A: Artificial neuron model; B: Background noise; C: Algorithm precision chart.

DISCUSSION

Semi-interactive detection algorithm of action potentials using local wave features and clustering combines two principles of detection of graphoelements: tracking of local features of a wave and clustering with subsequent selection of patterns. In certain parts, it is operator dependent. In our recordings, it attains sufficient accuracy and it can be efficiently employed for evaluation of non-stationary recordings of action potentials. Measured in the percentage of missed or misplaced spikes, our algorithm outperforms many other methods. However, this point of view is biased by the diversity of benchmarks used in establishing algorithm performance.

The development of waveform in time as a response to experimental intervention is the main subject of our research. Semi-interactive method for detection of action potentials allows us to observe changes in electrical activity (discharge frequency, coupling of discharges) of observed cells as a reaction to ischemia.

Neuronal death begins within 1 or 2 minutes after complete vascular occlusion in the core of the ischemic focus. Simultaneously, an area with gradually decreasing blood flow called penumbra develops around the ischemic core. Some neurons in penumbra become electrically inactive. These silent neurons may perish or recover. Our research revolves around changes in unit activity shortly before the activity disappears and in activity of surviving neurons. We assume that a change in activity of neurons synaptically connected with those in penumbra or in the core area

takes place. Therefore we evaluate unit activity of cortical neurons in contralateral hemisphere.

For routine evaluation, setup profiles for all adjustable constants will be necessary to implement in the program in order to introduce uniformity in the data processing and allow semi-skilled users to use it effectively. Our system is comparably as fast as marketed programs, however, its principal strength lies in effortless adjustability to a particular experiment.

REFERENCES

1. Pevsner PH, Eichenbaum JW, Miller DC, Pivawer G, Eichenbaum KD, Stern A, Zakian KL, Koutcher JA. A photothrombotic model of small early ischemic infarcts in the rat brain with histologic and MRI correlation. J Pharmacol Toxicol Methods 2001; 45 (3): 227-33.
2. Matejovska I, Bernaskova K, Krysl D, Mares J. Influence of melatonin pre-treatment and preconditioning by hypobaric hypoxia on the development of cortical photothrombotic ischemic lesion. Physiol Res 2007.
3. Watson BD, Dietrich WD, Busto R, Wachtel MS, Ginsberg MD. Induction of reproducible brain infarction by photochemically initiated thrombosis. Ann Neurol 1985; 17 (5): 497-504.
4. Yao H, Sugimori H, Fukuda K, Takada J, Ooboshi H, Kitazono T, Ibayashi S, Iida M. Photothrombotic middle cerebral artery occlusion and reperfusion laser system in spontaneously hypertensive rats. Stroke 2003; 34 (11): 2716-21.
5. Markgraf CG, Kraydieh S, Prado R, Watson BD, Dietrich WD, Ginsberg MD. Comparative histopathologic consequences of photothrombotic occlusion of the distal middle cerebral artery in Sprague-Dawley and Wistar rats. Stroke 1993; 24 (2): 286-92; discussion 292-3.
6. Lewicki MS. A review of methods for spike sorting: the detection and classification of neural action potentials. Network 1998; 9 (4): R53-78.
7. Bergman H, DeLong MR. A personal computer-based spike detector and sorter: implementation and evaluation. J Neurosci Methods 1992; 41 (3): 187-97.
8. Stewart CM, Newlands SD, Perachio AA. Spike detection, characterization, and discrimination using feature analysis software written in LabVIEW. Comput Methods Programs Biomed 2004; 76 (3): 239-51.
9. Andrew D, Craig AD. Responses of spinothalamic lamina I neurons to maintained noxious mechanical stimulation in the cat. J Neurophysiol 2002; 87 (4): 1889-901.
10. Rinberg D, Bialek W, Davidowitz H, Tishby N. Spike sorting in the frequency domain with overlap detection. Physics.data-an 2003; arXiv:physics/0306056v2: (Internet: http://arxiv.org/abs/physics/0306056).
11. Hulata E, Segev R, Ben-Jacob E. A method for spike sorting and detection based on wavelet packets and Shannon's mutual information. J Neurosci Methods 2002; 117 (1): 1-12.
12. Horn CC, Friedman MI. Detection of single unit activity from the rat vagus using cluster analysis of principal components. J Neurosci Methods 2003; 122 (2): 141-7.
13. Takahashi S, Anzai Y, Sakurai Y. Automatic sorting for multi-neuronal activity recorded with tetrodes in the presence of overlapping spikes. J Neurophysiol 2003; 89 (4): 2245-58.
14. Borisoff JF, McPhail LT, Saunders JT, Birch GE, Ramer MS. Detection and classification of sensory information from acute spinal cord recordings. IEEE Trans Biomed Eng 2006; 53 (8): 1715-9.
15. Brozovic M, Andersen RA. A nonparametric quantification of neural response field structures. Neuroreport 2006; 17 (10): 963-7.
16. Takahashi S, Anzai Y, Sakurai Y. A new approach to spike sorting for multi-neuronal activities recorded with a tetrode—how ICA can be practical. Neurosci Res 2003; 46 (3): 265-72.
17. Izhikevich EM. Simple Model of Spiking Neurons. IEEE Transactions On Neural Networks 2003; 14 (6): 1569-1572.

Aknowledgements: This work was supported by following grants: VZ 0021620816, GAUK 104/2004/C/3LF.

JOURNAL OF PHYSIOLOGY AND PHARMACOLOGY 2012, 63, 2, 127-132
www.jpp.krakow.pl

D. KRYSL[1,2], K. DEYKUN[1], L. LAMBERT[1], J. POKORNY[3], J. MARES[1]

PERIFOCAL AND REMOTE BLOOD-BRAIN BARRIER DISRUPTION IN CORTICAL PHOTOTHROMBOTIC ISCHEMIC LESION AND ITS MODULATION BY THE CHOICE OF ANESTHESIA

[1]Department of Normal, Pathological and Clinical Physiology, 3rd Faculty of Medicine, Charles University, Prague, Czech Republic;
[2]Department of Neurology, 2nd Faculty of Medicine, Motol Hospital, Charles University, Prague, Czech Republic;
[3]Department of Physiology, 1st Faculty of Medicine, Charles University, Prague, Czech Republic

We assessed blood-brain barrier (BBB) disruption in early stage of photothrombotic focal cerebral ischemia in the rat. We specifically looked for contralateral changes in BBB permeability and tested the influence of two anesthetics on the results. Adult Wistar rats were randomly anesthetized with pentobarbital (PB) or ketamine-xylazine (KX). Rats received intravenously (i.v.) Rose Bengal followed by Evans Blue (EB). Stereotactically defined spots on denuded skull were irradiated by laser (532 nm) for 18 min. Twenty four hours later, rats were killed, brains perfused, fixated, sectioned and slices analyzed by fluorescence microscopy. Volume of necrosis and volume of EB-albumin extravasation were calculated. Evidence of BBB breakdown in remote brain areas was sought and compared to sham handled controls. BBB disruption was consistently present, frequently with EB-albumin accumulating cells. Total lesion volume did not significantly differ among groups (TLV_{PB}=9.4±1.3 mm^3 *vs*. TLV_{KX}=8.3±2.1 mm^3); same was true for the volume of necrosis (NV_{PB}=5.1±0.7 mm^3 *vs*. NV_{KX}=6.3±1.9 mm^3). However, volume of EB-albumin extravasation area was significantly smaller in KX group ($EBEV_{PB}$=4.3±0.8 mm^3 *vs*. $EBEV_{KX}$=2.0±0.5 mm^3; p=0.0293). Median background EB-fluorescence signal density was higher in PB group (p<0.0001). Furthermore, regional increase in EB-fluorescence was found in two animals in PB group. Our study shows that anesthesia with NMDA-antagonist ketamine and α2-adrenergic agonist xylazine may reduce BBB breakdown in photothrombosis. Pentobarbital anesthesia lead to increased BBB permeability in the contralateral hemisphere.

Key words: *anesthesia, blood-brain barrier, cerebral ischemia, ketamine, pentobarbital, photothrombosis, stroke*

INTRODUCTION

Blood-brain barrier (BBB) permeability is altered in various pathological states, including ischemic stroke. Apart from being an important mechanism of secondary brain injury, BBB disruption with plasma protein extravasation was implied in late consequences of acute cerebral insults, namely epileptogenesis (1-4). The extent of BBB disruption differs among individual animal models of focal cerebral ischemia (5-9). Many factors contribute to this variability, including the choice of species, its vascular anatomy, capacity of collateral circulation, the duration of ischemia (transitory or permanent), the means of producing ischemia (large vessel occlusion, focal vasoconstriction, or microvascular occlusion, *e.g.* photothrombosis), and, possibly, the choice of anesthesia. Because BBB disruption in some models follows a biphasic course (10), the timing of evaluation becomes a major issue as well.

Usually, investigators focus on BBB disruption in the perilesional tissue. However, focal ischemia was shown to induce changes in the cerebral blood flow, brain metabolism and excitability also in remote functionally connected areas - a concept known as diaschisis (11-14). The possibility that diaschisis could include remote changes in BBB permeability was not tested.

In the present study, we evaluated perifocal, as well as contralateral BBB disruption in photochemically induced focal cerebral ischemia in rats. We also tested, whether the choice of anesthesia can influence the results.

MATERIAL AND METHODS

Adult Male Wistar albino rats (weight 200–220 g; ANLAB, Czech Republic) at postnatal day 60 and older were used. The animals were acclimated at least three days prior to the study and were maintained on a 12 hour light/dark cycle, with food and water available ad libitum. All experiments were performed in accordance with guidelines of the Ministry of Health, Czech Republic. Experimental protocols were approved by the Ethics committee of the 3rd Medical School, Charles University, Prague (Authorization No. for animal use: 17659/2007-30, issued on 9/7/2007; for numbers of funding grants see acknowledgements).

Experimental groups and anesthesia

Sixteen rats were randomly assigned in two experimental groups. Pentobarbital (20 mg/kg i.p.; Sigma, Czech Republic) was used for anesthesia in the first group ("PB"; N=8), a mixture of ketamine and xylazine (ketamine 80 mg/kg+xylazine 7 mg/kg i.p.; Sigma, Czech Republic) in the latter ("KX"; N=8). For comparison of background fluorescence signals, a sham-handled control group was created (N=4). Depth of anesthesia was tested at regular 5 min intervals by pressing the skin of the animal's hind-limb sole with anatomical tweezers. In case of hind-limb flexion, additional intraperitoneal bolus of half the calculated dose of ketamine was given to ensure surgical anesthesia. Usually, one additional dose of anaesthetic was needed prior to fixation of the animal in the stereotactic frame (approx. 20 minutes after the induction of anesthesia). Throughout the experiment, the animals did not show signs of respiratory distress, or other deficits in vital signs.

Surgery and photothrombosis

Photothrombosis was performed as previously described (15). After the induction of anesthesia, the scalp of the head was incised (2 cm length in midline) and the skull overlaying the left sensorimotor cortex was cleaned from soft tissues. A bolus of photosensitive dye Rose Bengal ("RB"-Sigma, Czech Republic; 20 mg/2 ml/kg, dissolved in 0.9% NaCl) was applied slowly into the systemic circulation *via* tail vein, followed by a bolus of Evans Blue ("EB"-Sigma, Czech Republic; 0.04 g/kg/2 ml; dissolved in 0.9% NaCl). After the application of dyes, the animals were positioned in a stereotactic frame. Next, three stereotactically defined adjacent points on the scull overlaying the hind-limb area of the left sensorimotor cortex were irradiated by a diode laser beam (532 nm; power density 50 mW/mm^2; illuminated area<1 mm^2). Each point was irradiated for 6 min (overall 18 min). After the end of photothrombosis, the animals were left to recover for 24 hours. In contrast to other tracers (*e.g.* natrium fluorescein), EB is almost completely bound to serum albumin. Thus, EB extravasation is a marker of albumin transport outside the blood vessels. We chose to apply EB prior to photothrombosis to mirror any change in BBB permeability within the first 24 hours of ischemia (from the onset of photothrombosis to brain perfusion and fixation).

Histology, image processing and evaluation

Twenty-four hours after photothrombosis, in deep urethane anesthesia, all animals were transcardially perfused with a solution of paraformaldehyde and decapitated. Brains were removed, fixated in paraformaldehyde and sectioned into 40 µm coronary slices. Lesion dimensions and the distribution of red fluorescence signal emitted by EB-albumin complex in green light were then studied with a fluorescence microscope (Olympus™). Digital microphotographs of all slices (both ipsilateral and contralateral cortex) were obtained at fixed image acquisition parameters (magnification, exposition, sensitivity, resolution, image format). Additional higher power microphotographs were acquired as needed. All digital photographs were then analyzed with a freely available utility ImageJ 1.37v (Wayne Rasband, National Institute of Health, USA; http://rsb.info.nih.gov/ij/).

1. Ischemic lesions and perifocal blood-brain barrier disruption

Area of necrosis was clearly delimited on each section (*Fig. 3*). With ImageJ tools, the area of necrosis was measured on each slice and multiplied by the thickness of the section – 40 µm. The sum of values from individual slices gave the volume of necrosis (NV) in an individual animal. The volume of EB-albumin extravasation (volume of BBB disruption) was measured similarly. The area of EB-albumin extravasation was delineated manually on each slide. Its border was defined as the point where clear increase in fluorescence signal was not anymore observable (*Fig 3A*). Again, the sum of values from individual slices gave the volume of EB-albumin extravasation (EBEV) in an individual animal. All measurements (608 slices in the PB group, 546 slices in the KX group) were performed by a single investigator (DK) to avoid inter-rater variability.

2. Remote blood-brain barrier disruption

BBB disruption in the contralateral hemisphere was evaluated by two methods. Firstly, all slices were visually examined for regions of increased fluorescence signal and for the occurrence of EB-positive cells (*i.e.* cells accumulating EB-

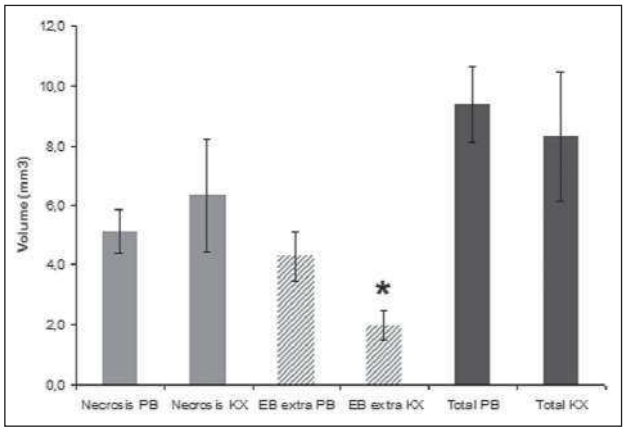

Fig. 1. Mean volumes of lesions in groups with different anesthesia. Values are presented as mean ±S.E.M. Mean volume of necrosis is shown in light gray, mean volume of EB-extravasation in hatched gray and mean total lesion volume in dark gray. In the group anesthetized with pentobarbital (n=8), the area of BBB disruption was significantly larger compared to ketamine-xylazine (n=8) group (p=0.0293, two-sided unpaired t-test).

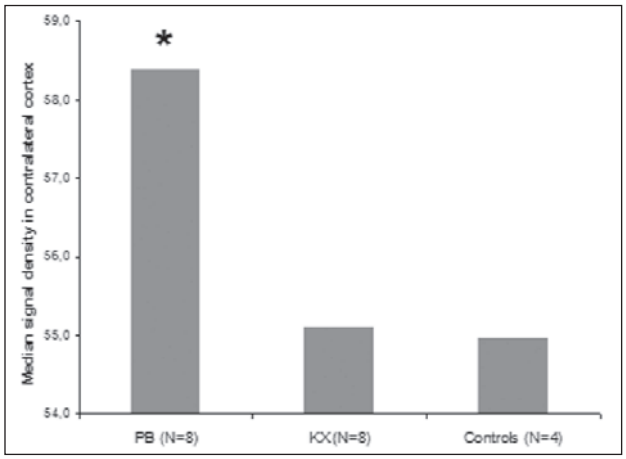

Fig. 2. Median EB-fluorescence signal density expressed as median gray value in a reference 1×2 mm section of the hemisphere contralateral to lesion. Median EB-fluorescence signal density was higher in PB group (p<0.0001, Kruskal-Wallis test with Dunn's Multiple Comparison Test). Median EB-fluorescence signal density in KX group was not different from controls.

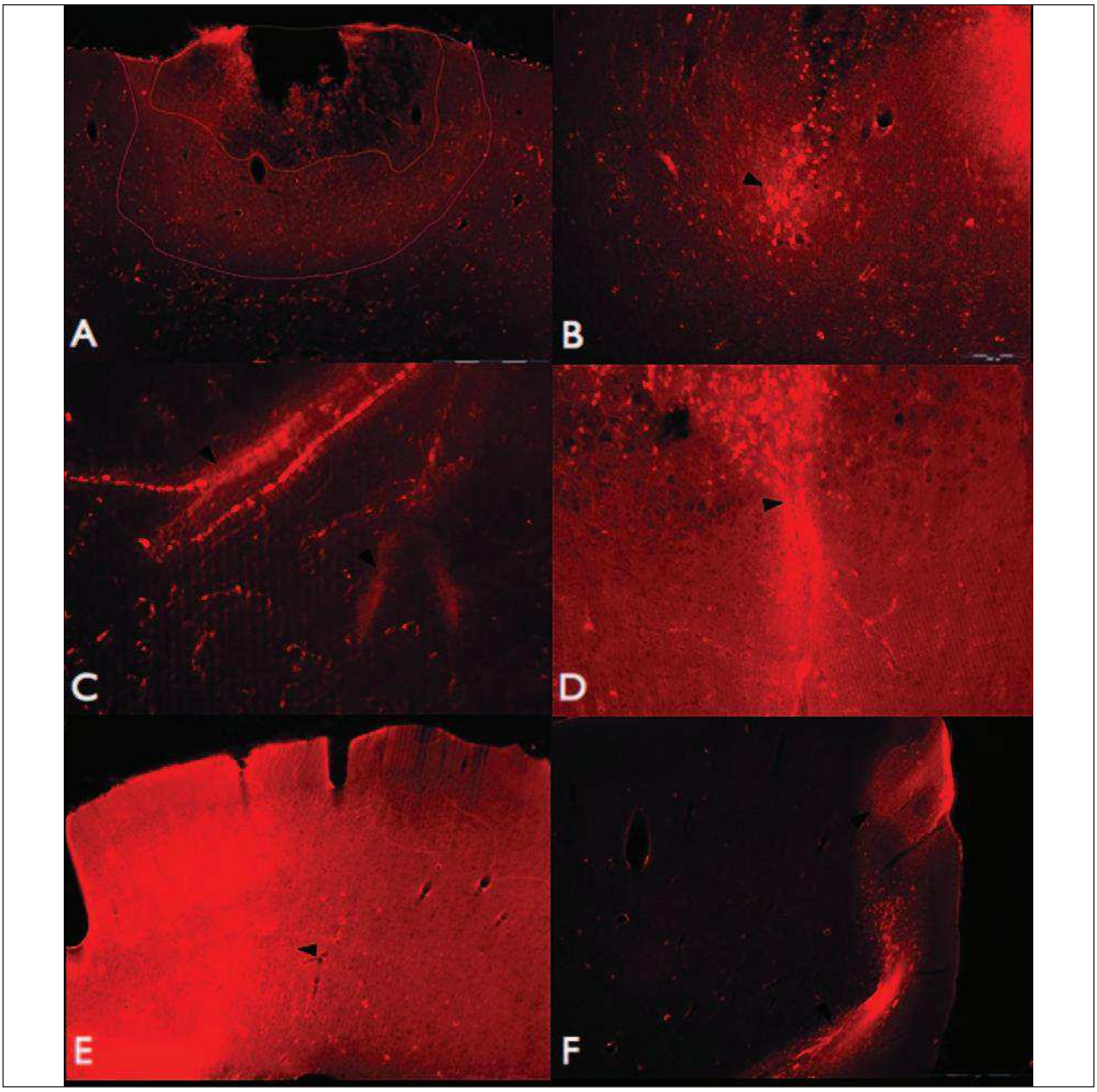

Fig. 3. Fluorescence microscopy images of the lesions. (*A*) Typical photochemically induced cortical ischemic lesion. Necrotic core can be seen with a surrounding brightly red area of extravasated EB-albumin. Lines denote the borders of necrotic core and the area of BBB disruption. The brightly red material (EB-albumin) in the cortical blood vessels can be seen in the lower half of the image. (*B*) A detailed view of the rim of necrosis and area of BBB failure. EB-albumin accumulating cells can be seen as bright red dots with a surrounding halo of EB-albumin extravasation (*black arrowheads*). (*C*) A larger blood vessel with EB-albumin adhering to its walls and escaping into the extracellular space (*black arrowheads*). (*D*) A detail view of the rim of the necrosis with EB-albumin accumulating cells and a blood vessel extending to the area of blood brain barrier alteration (*black arrowhead*). The extravasation of EB along the blood vessel walls is evident. (*E*) Low power image of the hemisphere contralateral to ischemic lesion (animal anesthetized with PB). A change in the background signal in the left half of the hemisphere (representing change in blood-brain-barrier permeability) can be noted (black arrowhead). (*F*) Signal changes in the medial part of the hemisphere contralateral to ischemic lesion (animal anesthetized with PB) (*black arrowheads*).

albumin complex). Secondly, we measured differences in background EB-fluorescence signal between the groups. In every sixth contralateral section, a virtual frame of 1×2 mm was placed on the contralateral cerebral cortex. The frame was consistently positioned in a "mirror" region corresponding to the contralateral area of ischemic lesion. Mean gray value (mean signal density) was measured within this region by ImageJ tools (mean gray value= the sum of the gray values of all the pixels in the selection divided by the number of pixels; in RGB images, each pixel was converted to gray-scale using the formula: gray=(red+green+blue)/3). Thus, we have obtained a set of mean gray values (mean signal densities) in all groups (PB, KX, controls). Differences between the groups were then statistically evaluated.

Statistical evaluation

GraphPad Prism 5.01 (GraphPad Software, Inc.) was used for statistical evaluation of the results. Normal distribution of the results was tested by D'Agostino&Pearson omnibus normality test. Statistical significance of differences between PB and KX group with respect to volume of necrosis and volume of EB-albumin extravasation were evaluated by unpaired t-test. Mean signal density values in the contralateral hemisphere were not normally distributed. Therefore, non-parametrical tests (Kruskal-Wallis test, and Mann-Whitney U test) were used to evaluate differences in this parameter among the groups.

RESULTS

Ischemic lesions with central area of necrosis were observed in all animals of both experimental groups 24 hours after photothrombosis (*Fig. 3A*). As a rule, a large area of EB-albumin extravasation surrounded the lesions, extending sometimes to the corpus callosum and subcortical structures. In some slices, brightly red EB-albumin accumulating cells were observed (*Fig. 3B-arrowhead*). Clusters of these cells were usually found at the border of the necrotic core and the area of BBB breakdown (*Fig. 3B, 3D*). EB-stained material was found in the blood vessels both in the ipsilateral and contralateral hemisphere and in subcortical structures (see *Fig. 3C, 3D-arrowhead*). Pial blood vessels, as well as perforating blood vessels perpendicular to the pial surface were sometimes found to be lined with EB-albumin complex. In larger vessels, EB-albumin complex was found adhering to the vessel wall and escaping into the extracellular space *(Fig. 3C*, *3D-arrowhead*).

Total volume of lesion (TLV; *i.e.* volume of necrosis + volume of EB-albumin extravasation) did not significantly differ between the groups (TLV_{PB}=9.4±1.3 mm^3 *vs.* TLV_{KX}=8.3±2.1 mm^3). The volume of necrosis (NV) was slightly larger in the ketamine-xylazine group (NV_{PB}=5.1±0.7 mm^3 *vs.* NV_{KX}=6.3±1.9 mm^3), however, the difference was not statistically significant. On the other hand, the volume of EB-albumin extravasation (EBEV) was significantly smaller in the KX group ($EBEV_{PB}$=4.3±0.8 mm^3 *vs.* $EBEV_{KX}$=2.0±0.5 mm^3; p=0.0293, two-sided unpaired t-test) (see *Fig. 1*).

Median EB-fluorescence signal density in the hemisphere contralateral to ischemic lesion was significantly increased in PB group ($p<0.0001$, Mann-Whitney U test). Median EB-fluorescence signal density in the K/X group was similar to the control group (*Fig. 2*). Moreover, in two animals from the pentobarbital group, diffuse changes in EB-fluorescence signal intensity were found in remote areas in the contralateral hemisphere (*Fig. 3E*, *3F-arrowheads*). Unequivocal EB-albumin accumulating cells were not found in the contralateral cortex.

DISCUSSION

The extent and anatomical pattern of BBB disruption differs among experimental models of focal ischemia. Breakdown of BBB to proteins is invariably present in transient middle cerebral artery occlusion (t-MCAO) (16-18), whereas it is not a typical feature of permanent occlusion model (p-MCAO) (6). Extensive perifocal vascular leakage is an important feature of photothrombosis (8), and it was shown to persist at least 24 hours after laser irradiation (19). In agreement with these findings, we have consistently observed areas of increased EB-albumin fluorescence surrounding necrotic core of ischemic lesions in the irradiated area. Areas of increased EB-fluorescence extended into the cerebral white matter and corpus callosum. Within these regions, we observed adherence of EB-positive material to the walls of larger penetrating vessels and its leakage into the extracellular space (*Fig. 3A-3D*). Apart from diffuse staining of the parenchyma surrounding the lesion core, we have observed uptake of EB-albumin complex into cells (*Fig. 3B, 3D-arrowheads*). Plasma protein uptake into brain cells was described in various models of focal brain ischemia, as well as other insults (20-25) and may play an important role in epileptogenesis (2-4). Interestingly, animals subject to photothrombosis (where large BBB breakdown is typical) frequently develop seizures (26-27).

Our study demonstrates that the extent of BBB disruption in the photothrombotic model can be significantly reduced when a combination of NMDA antagonist ketamine and α2-adrenoceptor agonist xylazine is used for anesthesia, in contrast to $GABA_A$ agonist pentobarbital. Similar results were observed when selective NMDA antagonist MK-801 was used in the t-MCAO model (28). We have found no direct evidence in the literature for xylazine-mediated alteration of blood-brain barrier permeability, although, in one study, a decrease of ethanol-induced BBB opening was observed following pretreatment with another α2-adrenoceptor agonist clonidine (29). On the other hand, the evidence for NMDA receptor mediated changes to BBB permeability is quite extensive (apart from other important pathophysiological roles of NMDA receptors, *e.g.* in excitotoxicity (30), memory consolidation, and mood disorders (31). NMDA stimulated uptake of HRP on isolated rat cerebral cappilaries (32), NMDA antagonist Hu-211 protects against BBB disruption in photothrombosis (33), intrastriatal injection of NMDA induced extravasation of Lucifer yellow and this extravasation was prevented by NMDA antagonist (34) and NMDA applied topically on the cortex increased BBB permeability (35). Nevertheless, it must be noted, that in some models, this effect of NMDA receptor blockade on BBB permeability was not reproduced (36).

Although we cannot rule out the role of xylazine in producing the observed effects, we suggest that the presented evidence favors the main role of ketamine in the observed results. The mechanism of NMDA-receptor mediated regulation of BBB permeability remains to be elucidated. Other investigators observed glutamate-induced changes in expression, phosphorylation and distribution of tight-junction proteins, such as occludin (37). Increased transcellular transport of EB-albumin complex in a receptor mediated fashion is also possible (4).

Apart from evaluating perilesional changes in BBB integrity, we also tested whether focal ischemic lesion can induce BBB alteration in remote (but functionally connected) areas (diaschisis). The median background EB-fluorescence signal density was significantly increased in the pentobarbital group (*Fig. 2*), compared to KX and controls. Furthermore, in two animals from the PB group, we have found regional increase in EB-fluorescence signal density in the medial part of the contralateral hemisphere (*Fig. 3E*, *3F-arrowheads*). Also, in our preliminary experiments in animals anesthetized with PB, we have observed occasional cellular uptake of EB-albumin in the cerebellum. Although limited, these findings may support the possibility that the concept of diaschisis is also relevant to the regulation of permeability of blood-brain barrier and that alteration of neurotransmission may be involved.

The main limitation of our study is the absence of blood pressure monitoring throughout the experiment. However, with the intraperitoneal route of administration, the risk of hypotension is probably lower than with i.v. application. Moreover, episodes of hypotension would probably tend to influence the results in favor of pentobarbital as in the work by Chi *et al*. (38), which was not the case in our study.

In summary, our study shows that anesthesia with NMDA receptor antagonist ketamine decreases the extent of BBB breakdown in cortical photothrombosis. Furthermore, our results indicate that alteration of blood-brain barrier at sites contralateral to photochemically induced ischemic lesion is possible and that it may also be related to the choice of anesthesia. Further studies are needed to broaden these potentially clinically relevant observations.

Acknowledgements: The work was supported by following grants: Charles Univesity Pregue, research project UNCE204010; Charles Univesity Pregue, 264706/SVV/2012; Ministry of Education, Youth and Sports CMS 110/2012.

Conflict of interests: None declared.

REFERENCES

1. Cornford EM, Oldendorf WH. Epilepsy and the blood-brain barrier. *Adv Neurol* 1986; 44: 787-812.
2. Seiffert E, Dreier JP, Ivens S, *et al.* Lasting blood-brain barrier disruption induces epileptic focus in the rat somatosensory cortex. *J Neurosci* 2004; 24: 7829-7836.
3. Bolwig TG. Blood-brain barrier studies with special reference to epileptic seizures. *Acta Psychiatr Scand Suppl* 1988; 345: 15-20.
4. Ivens S, Kaufer D, Flores LP, *et al*. TGF-beta receptor-mediated albumin uptake into astrocytes is involved in neocortical epileptogenesis. *Brain* 2007; 130: 535-547.
5. Hossmann KA, Olsson Y. The effect of transient cerebral ischemia on the vascular permeability to protein tracers. *Acta Neuropathol* 1971; 18: 103-112.
6. Olsson Y, Crowell RM, Klatzo I. The blood-brain barrier to protein tracers in focal cerebral ischemia and infarction caused by occlusion of the middle cerebral artery. *Acta Neuropathol* 1971; 18: 89-102.
7. Coyle P. Middle cerebral artery occlusion in the young rat. *Stroke* 1982; 13: 855-859.
8. Dietrich WD, Busto R, Watson BD, Scheinberg P, Ginsberg MD. Photochemically induced cerebral infarction. II. Edema and blood-brain barrier disruption. *Acta Neuropathol* 1987; 72: 326-334.
9. Hughes PM, Anthony DC, Ruddin M, *et a*l. Focal lesions in the rat central nervous system induced by endothelin-1. J Neuropathol Exp Neurol 2003; 62: 1276-1286.
10. Kuroiwa T, Ting P, Martinez H, Klatzo I. The biphasic opening of the blood-brain barrier to proteins following temporary middle cerebral artery occlusion. *Acta Neuropathol* 1985; 68: 122-129.
11. Hossmann KA, Schuier FJ. Experimental brain infarcts in cats. I. Pathophysiological observations. *Stroke* 1980; 11: 583-592.
12. Kataoka K, Hayakawa T, Yamada K, Mushiroi T, Kuroda R, Mogami H. Neuronal network disturbance after focal ischemia in rats. *Stroke* 1989; 20: 1226-1235.
13. Izumi Y, Haida M, Hata T, Isozumi K, Kurita D, Shinohara Y. Distribution of brain oedema in the contralateral hemisphere after cerebral infarction: repeated MRI measurement in the rat. *J Clin Neurosci* 2002; 9: 289-293.
14. Buchkremer-Ratzmann I, August M, Hagemann G, Witte OW. Electrophysiological transcortical diaschisis after cortical photothrombosis in rat brain. *Stroke* 1996; 27: 1105-1109, discussion 1109-1111.
15. Matejovska I, Bernaskova K, Krysl D, Mares J. Influence of melatonin pretreatment and preconditioning by hypobaric hypoxia on the development of cortical photothrombotic ischemic lesion. *Physiol Res* 2008; 57: 283-288.
16. Yang GY, Betz AL. Reperfusion-induced injury to the blood-brain barrier after middle cerebral artery occlusion in rats. *Stroke* 1994; 25: 1658-1664, discussion 1664-1665.
17. Huang ZG, Xue D, Preston E, Karbalai H, Buchan AM. Biphasic opening of the blood-brain barrier following transient focal ischemia: effects of hypothermia. *Can J Neurol Sci* 1999; 26: 298-304.
18. Nagaraja TN, Keenan KA, Fenstermacher JD, Knight RA. Acute leakage patterns of fluorescent plasma flow markers after transient focal cerebral ischemia suggest large openings in blood-brain barrier. *Microcirculation* 2008; 15: 1-14.
19. Hoff EI, oude Egbrink MG, Heijnen VV, Steinbusch HW, van Oostenbrugge RJ. In vivo visualization of vascular leakage in photochemically induced cortical infarction. *J Neurosci Methods* 2005; 141: 135-141.
20. Loberg EM, Karlsson BR, Torvik A. Neuronal uptake of plasma proteins after transient cerebral ischemia/hypoxia. Immunohistochemical studies on experimental animals and human brains. *APMIS* 1993; 101: 777-783.
21. Loberg EM, Torvik A. Neuronal uptake of plasma proteins in brain contusions. An immunohistochemical study. *Acta Neuropathol* 1992; 84: 234-237.
22. Remmers M, Schmidt-Kastner R, Belayev L, Lin B, Busto R, Ginsberg MD. Protein extravasation and cellular uptake after high-dose human-albumin treatment of transient focal cerebral ischemia in rats. *Brain Res* 1999; 827: 237-242.
23. Sokrab TE, Kalimo H, Johansson BB. Parenchymal changes related to plasma protein extravasation in experimental seizures. *Epilepsia* 1990; 31: 1-8.
24. Matz PG, Lewen A, Chan PH. Neuronal, but not microglial, accumulation of extravasated serum proteins after intracerebral hemolysate exposure is accompanied by cytochrome c release and DNA fragmentation. *J Cereb Blood Flow Metab* 2001; 21: 921-928.
25. Murakami K, Kawase M, Kondo T, Chan PH. Cellular accumulation of extravasated serum protein and DNA fragmentation following vasogenic edema. *J Neurotrauma* 1998; 15: 825-835.
26. Kelly KM, Kharlamov A, Hentosz TM, *et al.* Photothrombotic brain infarction results in seizure activity in aging Fischer 344 and Sprague Dawley rats. *Epilepsy Res* 2001; 47: 189-203.
27. Kharlamov EA, Jukkola PI, Schmitt KL, Kelly KM. Electrobehavioral characteristics of epileptic rats following photothrombotic brain infarction. *Epilepsy Res* 2003; 56: 185-203.
28. Yang G, Chan PH, Chen SF, Babuna OA, Simon RP, Weinstein PR. Reduction of vasogenic edema and infarction by MK-801 in rats after temporary focal cerebral ischemia. *Neurosurgery* 1994; 34: 339-345, discussion 345.
29. Borisenko SA. Effects of drugs on blood-brain barrier permeability in rats chronically intoxicated by ethanol. *Ann Ist Super Sanita* 1990; 26: 39-42.
30. Wyrembek P, Szczuraszek K, Majewska MD, Mozrzymas JW. Intermingled modulatory and neurotoxic effects of thimerosal and mercuric ions on electrophysiological responses to GABA and NMDA in hippocampal neurons. *J Physiol Pharmacol* 2010; 61: 753-758.
31. Lehner M, Wislowska-Stanek A, Skorzewska A, *et al*. Expression of N-methyl-D-aspartate (R)(GluN2B) - subunits in the brain structures of rats selected for low and high anxiety. *J Physiol Pharmacol* 2011; 62: 473-482.
32. Koenig H, Trout JJ, Goldstone AD, Lu CY. Capillary NMDA receptors regulate blood-brain barrier function and breakdown. *Brain Res* 1992; 588: 297-303.

33. Belayev L, Busto R, Watson BD, Ginsberg MD. Post-ischemic administration of HU-211, a novel non-competitive NMDA antagonist, protects against blood-brain barrier disruption in photochemical cortical infarction in rats: a quantitative study. *Brain Res* 1995; 702: 266-270.
34. Miller RD, Monsul NT, Vender JR, Lehmann JC. NMDA- and endothelin-1-induced increases in blood-brain barrier permeability quantitated with Lucifer yellow. *J Neurol Sci* 1996; 136: 37-40.
35. Chi OZ, Chang Q, Weiss HR. Effects of topical N-methyl-D-aspartate on blood-brain barrier permeability in the cerebral cortex of normotensive and hypertensive rats. *Neurol Res* 1997; 19: 539-544.
36. Preston E, Webster J, Palmer GC. Lack of evidence for direct involvement of NMDA receptors or polyamines in blood-brain barrier injury after cerebral ischemia in rats. *Brain Res* 1998; 813: 191-194.
37. Andras IE, Deli MA, Veszelka S, Hayashi K, Hennig B, Toborek M. The NMDA and AMPA/KA receptors are involved in glutamate-induced alterations of occludin expression and phosphorylation in brain endothelial cells. *J Cereb Blood Flow Metab* 2007; 27: 1431-1443.
38. Chi OZ, Chun TW, Liu X, Weiss HR. The effects of pentobarbital on blood-brain barrier disruption caused by intracarotid injection of hyperosmolar mannitol in rats. *Anesth Analg* 1998; 86: 1230-1235.

Received: October 16, 2011
Accepted: March 28, 2012

Author's address: Dr. David Krysl, Department of Normal, Pathological and Clinical Physiology, 3rd Faculty of Medicine, Charles University, 4 Ke Karlovu Street, 120 00 - Prague 2, Czech Republic; Phone: +420 224 923 241; E-mail: dkrysl@gmail.com